



# Determination of the interior pH of lipid nanoparticles using a pH-sensitive fluorescent dye-based DNA probe

Bin Zhao<sup>a,\*</sup>, Albert Kamanzi<sup>b</sup>, Yao Zhang<sup>b,c</sup>, Karen Y.T. Chan<sup>a</sup>, Madelaine Robertson<sup>a</sup>, Sabrina Leslie<sup>b</sup>, Pieter R. Cullis<sup>a,\*\*</sup>

<sup>a</sup> Department of Biochemistry and Molecular Biology, University of British Columbia, Vancouver, British Columbia, V6T 1Z4, Canada

<sup>b</sup> Michael Smith Laboratories and Department of Physics, University of British Columbia, Vancouver, British Columbia, V6T 1Z4, Canada

<sup>c</sup> School of Biomedical Engineering, University of British Columbia, Vancouver, British Columbia, V6T 1Z4, Canada

## ARTICLE INFO

### Keywords:

Lipid nanoparticles  
Ionizable cationic lipids  
pH-sensitive dye  
Fluorescent DNA probes  
Single-particle imaging  
siRNA therapeutics

## ABSTRACT

Lipid nanoparticles (LNPs) containing ionizable cationic lipids are proven delivery systems for therapeutic nucleic acids, such as small interfering RNA (siRNA). It is important to understand the relationship between the interior pH of LNPs and the pH of the external environment to understand LNP formulation and function. Here, we developed a simple and rapid approach for determining the pH of the LNP core using a pH-sensitive fluorescent dye-based DNA probe. LNP siRNA systems containing pH-responsive DNA probes (LNP-siRNA&DNA) were generated by rapid mixing of lipids in ethanol and pH 4 aqueous buffer containing siRNA and DNA probes. We demonstrated that DNA probes were readily encapsulated in LNP systems and were sequestered into an environment at a high concentration as evidenced by an inter-probe FRET signal. It was shown that the pH of LNP encapsulated probes closely follows the pH increase or decrease of the external environment. This indicates that the clinically approved LNP RNA systems with similar lipid compositions (e.g., Onpattro and Comirnaty) are highly permeable to protons and that the pH of the interior environment closely mirrors the external environment. The pH-dependent response of the probe in LNPs was also confirmed under buffer conditions at various pHs. Furthermore, we showed that the pH-sensitive DNA probe can be incorporated into LNP systems at levels that allow the pH response to be monitored at a single LNP level using convex lens-induced confinement (CLiC) confocal microscopy. Direct visualization of the internal pH of single particles with the fluorescent DNA probe was achieved by CLiC for LNP-siRNA&DNA systems formulated under both high and normal ionic strength conditions.

## 1. Introduction

Small interfering RNA (siRNA) and messenger RNA (mRNA)-based therapeutics enabled by lipid nanoparticle (LNP) delivery systems hold great promise for treating cancer, hereditary genetic disorders, and neurological and infectious diseases (Cheng et al., 2022; Hu et al., 2020; Witzigmann et al., 2020). The clinical potential of LNP RNA systems was first demonstrated by the LNP siRNA formulation, Patisiran (Onpattro), which was approved as a novel treatment for transthyretin-mediated amyloidosis (Adams et al., 2018; Akinc et al., 2019; Kulkarni et al., 2019a). The subsequent global success of the LNP mRNA COVID-19 vaccines (e.g., Comirnaty developed by Pfizer-BioNTech) has greatly amplified interest in developing LNP RNA therapeutics (Han et al., 2021;

Kulkarni et al., 2018; Semple et al., 2010; Sun and Lu, 2023). These LNP RNA formulations contain ionizable cationic lipids, which are positively charged at acidic pH to allow the entrapment of negatively charged nucleic acids, but are neutral at physiological pH to minimize cytotoxicity. Furthermore, protonation of the ionizable lipids in the acidic endosome following uptake into cells can promote electrostatic interactions between the LNPs and the endosomal membrane. These interactions have been proposed to disrupt the endosomal membrane, leading to the release of nucleic acid cargos into the cytoplasm (Hafez et al., 2001; Han et al., 2021). Previous studies have estimated that less than 2 % of siRNA can escape the endosome and reach the cytosol for LNP-mediated siRNA delivery (Gilleron et al., 2013; Zheng et al., 2023). However, the precise details whereby endocytic pH regulates endosome

\* Corresponding author.

\*\* Corresponding author.

E-mail addresses: [zbsinap@gmail.com](mailto:zbsinap@gmail.com), [bin.zhao@ubc.ca](mailto:bin.zhao@ubc.ca) (B. Zhao), [pieterc@mail.ubc.ca](mailto:pieterc@mail.ubc.ca) (P.R. Cullis).

<https://doi.org/10.1016/j.bios.2024.116065>

Received 24 November 2023; Received in revised form 15 January 2024; Accepted 22 January 2024

Available online 24 January 2024

0956-5663/© 2024 Elsevier B.V. All rights reserved.

escape of RNA entrapped in ionizable LNPs remain unclear.

It is important to develop an analytical tool to directly monitor the pH microenvironment experienced by ionizable lipids in LNPs during endocytosis. In addition, previous work indicates that during LNP formation, as the pH is raised from 4 to 7.4, the ionizable cationic lipids adopt a neutral form which promotes the fusion of small vesicles (formed at pH 4) into larger particles with amorphous “oil droplet” or “solid core” electron-dense cores at pH 7.4 (Kulkarni et al., 2018). However, there is no direct evidence that the interior of the LNP reflects the outer environment during this process. Again, a simple and rapid method for the monitoring of the pH microenvironment of ionizable lipids in LNPs is required.

DNA-based fluorescent probes are powerful tools for analytical and biological applications (Huang et al., 2021; Juskowiak, 2011; Keshri et al., 2021; Zhao et al., 2017), including pH sensing and cellular pH mapping (Amodio et al., 2014; Modi et al. 2009, 2013). Furthermore, it is likely that such probes can be efficiently entrapped into LNPs given the efficient encapsulation of a variety of negatively charged macromolecules, including siRNA, antisense oligonucleotides, and mRNA (Leung et al., 2015). Thus, a pH-sensitive dye-conjugated DNA probe could provide a strategy for directly monitoring the pH microenvironment of ionizable lipids inside LNPs. 6-Carboxyfluorescein (6-FAM), a derivative of fluorescein, has been widely used as a pH indicator in living cells due to its favorable spectral properties, reversible pH sensitivity, good photostability, and low leaking rate through the cell membrane (Le Guern et al., 2020). In addition, 6-FAM-DNA conjugates can be synthesized in a single step, and are inexpensive and easy to use.

In this work, we used 6-FAM as a pH-sensitive dye to develop a fluorescent DNA probe for the direct monitoring of the pH microenvironment that ionizable lipids in LNPs are exposed to. The dual-labeled fluorescent DNA probe was designed by conjugating 6-FAM and Alexa Fluor 647 (a pH-insensitive dye used as an internal reference) to the DNA duplex. LNP-siRNA&DNA systems were then constructed by co-encapsulating the pH-sensitive dye-based DNA probe with siRNA into LNPs. We demonstrated that the DNA probe could indicate the pH change inside LNPs in response to the pH change of the external buffer. The pH-dependent response of the probe was investigated under a range of pH conditions, and we demonstrated that the pH probe was associated with the LNPs by the presence of a FRET signal and by imaging single LNPs using convex lens-induced confinement (CLiC) confocal microscopy.

## 2. Materials and methods

### 2.1. Materials

The ionizable lipid, DLin-MC3-DMA (MC3), was synthesized by the lab of Dr. Marco Ciufolini. The lipids, DSPC and PEG-DMG, were purchased from Avanti Polar Lipids. All other chemicals were purchased from Sigma Aldrich unless otherwise stated. All DNA oligonucleotides were synthesized and purified by Integrated DNA Technologies. DNA sequence (5'-3') are as follows:

O1-6FAM: 6-FAM - TACATTTTACGCCTGGTGCCT  
 O2-A647: CCGACCGCAGGATCCTATAA - Alexa Fluor 647  
 O3: TTATAGGATCTGCGGTCGGAGGCACCAGGCGTAAATGTA

All the experiments were repeated three times, unless otherwise specified.

### 2.2. DNA probe preparation

All DNA oligonucleotides, including O1-6FAM, O2-A647 and O3, were mixed in 100  $\mu$ L PBS at a concentration of 5  $\mu$ M. The resulting mixture was first heated to 90  $^{\circ}$ C for 5 min and then cooled to 25  $^{\circ}$ C at a rate of 5  $^{\circ}$ C/15 min using a MJ Research PTC-200 Thermal Cycler. The

assembled DNA probe was stored at 4  $^{\circ}$ C until usage.

### 2.3. LNP formulation and characterization

LNP-siRNA&DNA systems were formulated as previously described (Cheng et al., 2023; Kulkarni et al., 2019b), with slight modifications. All formulations were formulated by first dissolving lipids (DLin-MC3-DMA, Cholesterol, PEG-DMG and DSPC) into ethanol to a final concentration of 10 mM and at a ratio of 50/38.5/1.5/10 mol%, respectively. The lipid mixture was then rapidly mixed with an aqueous solution of siRNA and fluorescent DNA probes (at a 9:1 or 1:1 wt ratio) in NaOAc-NaCl (25 mM sodium acetate, 150 mM sodium chloride) pH 4 or NaOAc (25 mM sodium acetate) pH 4 buffer using a T-junction mixer at a 1:3 ethanol/aqueous buffer ratio (v/v) and a final flow rate of 20 mL  $\text{min}^{-1}$ . The amine-to-phosphate ratio (N/P) was 3. The resulting mixture was dialyzed overnight against >500-fold volume of various buffers (NaOAc-NaCl pH 4 buffer, pH 7.4 PBS, pH 4, 5, 6 or 7 citrate-phosphate buffer). The prepared LNPs were then sterile-filtered with a 0.2  $\mu$ m Supor membrane syringe filter (Pall Corporation, Mississauga, ON, Canada) and concentrated in 30K Amicon ultracentrifugation units (EMD Millipore Corporation, Billerica, MA, USA). Total lipid content was calculated using the cholesterol concentration measured by a Cholesterol E Kit (Wako Diagnostics, Mountain View, CA, USA). Particle size (number mean) was measured via dynamic light scattering using a Malvern Zetasizer Nano ZS instrument.

To quantify the encapsulation efficiency of total nucleic acids (siRNA and DNA) in LNPs, the same DNA probe without dye modification prepared using unmodified oligonucleotides was co-encapsulated with siRNA into LNPs as described above. Then the Quant-iT RiboGreen RNA Assay Kit (Wako Diagnostics, Mountain View, CA, USA) was used to quantify the encapsulation efficiency of total nucleic acids, in which the RiboGreen reagent (Excitation: 500nm/ Emission: 525 nm) shows bright green fluorescence upon binding to RNA or DNA. Triton X-100 can lyse the LNPs to release the encapsulated nucleic acids. The sum amount of siRNA and DNA used in the formulation was determined by treating the formulation with 1 % (v/v) Triton X-100 and incubating with Ribogreen reagent at room temperature for 5 min. The amount of un-encapsulated nucleic acids (siRNA and DNA) was determined by directly incubating the formulation with Ribogreen reagent at room temperature for 5 min. The encapsulation efficiency of total nucleic acids was calculated by subtracting the amount of un-encapsulated nucleic acids (siRNA and DNA) from the sum amount of siRNA and DNA used in the formulation, and dividing by the sum amount of siRNA and DNA used in the formulation.

### 2.4. pH assays and fluorescence measurements

Fluorescence measurements were performed with a PerkinElmer LS 55 Fluorescence Spectrometer. The excitation wavelength of 6-FAM and Alexa Fluor 647 was 488 nm and 640 nm respectively. The emission spectra at the ranges of 510–750 nm and 650–760 nm were collected for each fluorophore. A length of 5 nm was set for both the excitation and emission slits. To test the particles' behavior during pH increase, LNP-siRNA&DNA samples formulated and dialyzed against NaOAc-NaCl pH 4 buffer were diluted 10 times with pH 7.4 PBS, followed by fluorescence measurements. To lyse the particles, Triton X-100 was added to the diluted samples to a final concentration of 1 % (v/v). For buffer acidification, 0.1 N HCl was added to the diluted samples to lower the pH from 6.8 to 4. Alternatively, LNP samples (prediluted 10 times with pH 7.4 PBS) were diluted 5 times with NaOAc-NaCl pH 4 buffer until the final pH was 5.

### 2.5. CLiC imaging

The CLiC imaging device holds a flow cell constructed by a top glass coverslip (25 mm  $\times$  25 mm, 150  $\pm$  20  $\mu$ m-thick) containing an array of

embedded posts and a bottom glass coverslip (25 mm × 25 mm, 200 ± 10 μm-thick) containing an array of embedded microwells (Kamanzi et al., 2021). A deep micro-channel was present for the exchange of reagents. The array of posts (post diameter: 10 μm, depth: 20 nm), microwells (microwell diameter: 3 μm, depth: 500 nm), and the micro-channel were patterned by standard photolithography. This was followed by dry-etching of the microwells and posts using a reactive ion etching (RIE) technique, while the micro-channel was patterned using wet etching with hydrofluoric acid (Henkin et al., 2016). Both the top and bottom coverslips were passivated with polyethylene glycol (PEG) layers using silane chemistry, an amine-thiol cross-linker, and a click point PEGylation technique previously described in the literature (Emilsson et al., 2015; Kamanzi et al., 2021). The assembled flow cell was sealed in a custom microfluidic chuck for imaging.

The microscopy setup and imaging process were performed as previously described (Kamanzi et al., 2021). In short, the CLiC lens was controlled by a nanopositioner to a lowered position to deflect the top layer of the flow cell downward. This confined the suspension of particles within the array of microwells. A 100 × oil immersion objective lens (Apochromat TIRF 100 × oil immersion objective lens N.A. 1.49, W.D. 0.12 mm, F.O.V 22 mm) was used to image the particles. The LNP samples were excited by a 488 nm Coherent Sapphire LP laser and a 647 nm Coherent Obis laser. Optimal emission filter settings were used for 6-FAM (525 ± 50 nm, part number: Chroma ET525/50m) and Alexa Fluor 647 (680 ± 40 nm, part number: Chroma ET680/40m) to minimize the fluorescence bleed-through. The exposure time and laser power were 20 ms and 0.5 mW, respectively. Data analysis was performed by a

MATLAB-based single particle tracking software developed in the lab.

### 3. Results

#### 3.1. Probe design and LNP formulation

The DNA duplex-based fluorescent probe developed here was composed of three oligonucleotides (Fig. 1A), O1, O2 and O3, in which O1 and O2 were labeled with 6-FAM and Alexa Fluor 647 respectively. 6-FAM exhibited excellent pH sensitivity between pH 4 to pH 7.4 (Figure S1), while the fluorescent signal from Alexa Fluor 647 was stable across this pH range, which allowed the fluorophore to act as an internal standard. Due to the relatively long distance (>10 nm) between the two dyes, with a theoretical distance of 41 base pairs (approximately 14 nm), no intramolecular FRET signals were observed. The sensing mechanism of the fluorescent pH probe is based on the excellent pH sensitivity of 6-FAM. As a derivative of fluorescein (Le Guern et al., 2020), similarly, the ionic charge and chemical structure of 6-FAM vary with its surrounding pH, leading to fluctuations of the photophysical properties. Under basic conditions, 6-FAM exhibits a very high fluorescence quantum yield when excited at 488 nm, but the fluorescence gradually diminishes as the solution becomes more acidic. This fluctuation is attributed to the transition of the di/tri-anionic form of 6-FAM into a mono-anionic equilibrium. At pH 4, the 6-FAM fluorescence was undetectable ("Inactivated state") under irradiation at 488 nm because it was in a mono-anionic or neutral form. When the pH was raised to neutral, the most fluorescent di/tri-anionic form of 6-FAM took prominence over

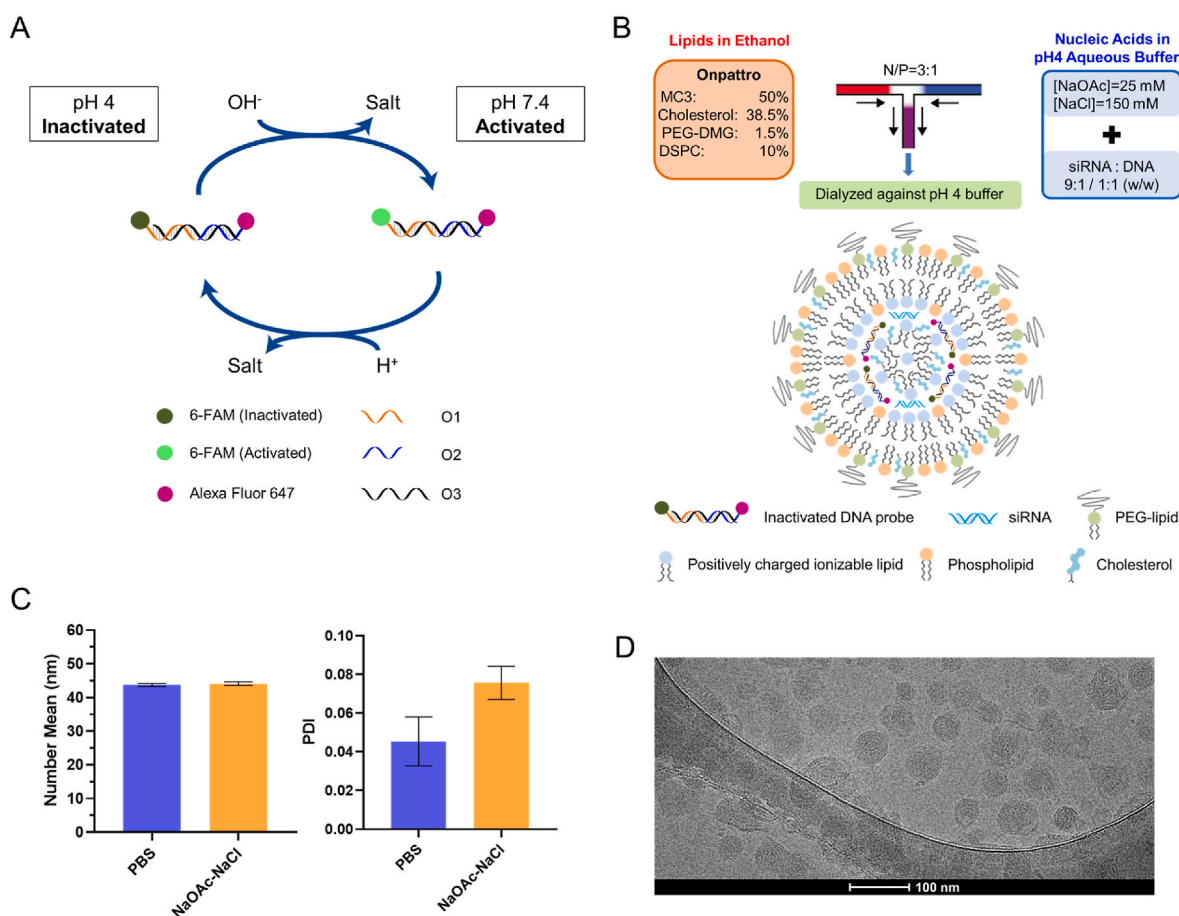


**Fig. 1.** pH-sensitive dye-based DNA probe and LNP-siRNA&DNA formulation. (A) Schematic of the DNA-based fluorescent pH sensor. (B) Workflow of the LNP-siRNA&DNA formulation. (C) Particle size (number mean, left) and polydispersity index (PDI, right) of LNP-siRNA&DNA measured by dynamic light scattering (DLS). NaOAc-NaCl refers to particles formulated and dialyzed against NaOAc-NaCl pH 4 buffer, PBS stands for control particles formulated with NaOAc-NaCl pH 4 buffer and dialyzed against PBS (pH 7.4). (D) CryoTEM image of LNP-siRNA&DNA (pH 4). Particles were formulated and dialyzed against NaOAc-NaCl pH 4 buffer.

other forms (“Activated state”), leading to strong fluorescence visualized as a peak at 520 nm.

LNPs with the Onpattro lipid composition (DLin-MC3-DMA, Cholesterol, PEG-DMG, DSPC at a molar composition of 50/38.5/1.5/10) were formulated by rapid T-tube mixing of the lipids dissolved in ethanol with the aqueous buffer at pH 4 (Fig. 1B). Note there are two ways of formulating LNP RNA systems-either using pH 4 buffers with low ionic strength such as 25 mM sodium acetate (NaOAc) (Kulkarni et al., 2018) or using pH 4 buffers with high ionic strength such as 300 mM NaOAc or sodium citrate (Cheng et al., 2023). The use of buffers with high ionic strength induces fusion between the small vesicles that form on dispersions of lipids in ethanol into an aqueous medium (Batzri and Korn, 1973), reaching a size limited by the PEG-lipid content, whereas the use of buffers with a low ionic strength results in small vesicles that fuse as the pH is raised on dialysis against PBS, again reaching a size dictated by the PEG-lipid content (Kulkarni et al., 2018). Here, as we wished to characterize formed LNP RNA systems both at pH 4 and pH 7.4, we chose to use a high ionic strength NaOAc-NaCl (25 mM sodium acetate, 150 mM sodium chloride) pH 4 buffer. The size and morphology of the LNP-siRNA&DNA systems produced using the NaOAc-NaCl pH 4 buffer were characterized by dynamic light scattering (DLS) and cryogenic transmission electron microscopy (CryoTEM). After dialysis against NaOAc-NaCl pH 4 buffer to remove ethanol, the particle size was ~45 nm (Fig. 1C), similar to that of particles formed in NaCl-free NaOAc (25 mM sodium acetate) pH 4 buffer and dialyzed against PBS (pH 7.4) (Kulkarni et al., 2018). CryoTEM images showed

that the LNP-siRNA&DNA exhibited the expected electron-dense core structures at both pH 4 and pH 7.4 (Fig. 1D, Figure S2). The encapsulation efficiency of total nucleic acids was estimated to be 85 % by the RiboGreen assay. A gel mobility shift assay (Figure S3) showed that no free DNA probe was detectable and further confirmed the high encapsulation efficiency of DNA probes in LNPs.

### 3.2. Activation of LNP-siRNA&DNA in response to pH increases

We first asked if the encapsulated fluorescent DNA pH probe can respond to a pH increase in the external buffer. At pH 4, when excited at 488 nm, the probe showed non-detectable signals for 6-FAM; however, an emission peak of 6-FAM at 520 nm was observed when the pH was raised to 6.8 by diluting samples 10 times with PBS (Fig. 2A). Most interestingly, another peak appeared at 670 nm, suggesting a FRET interaction between 6-FAM and Alexa Fluor 647 in LNPs. Given that such a FRET signal was not detected for the free probe (Figure S1), this signal likely arose from an inter-probe interaction between 6-FAM and Alexa Fluor 647 when 6-FAM became activated at pH 6.8. To confirm this hypothesis, the LNPs were treated with Triton X-100 which would lyse the LNPs to release the encapsulated nucleic acids. The signal of 6-FAM at 520 nm increased dramatically, which could be attributed to the elimination of the self-quenching effects as the dye was no longer confined within the core of the LNP. Most importantly, the FRET peak at 670 nm disappeared as the LNPs were lysed, confirming that the integrity of LNPs was essential to the FRET effects and the FRET indeed

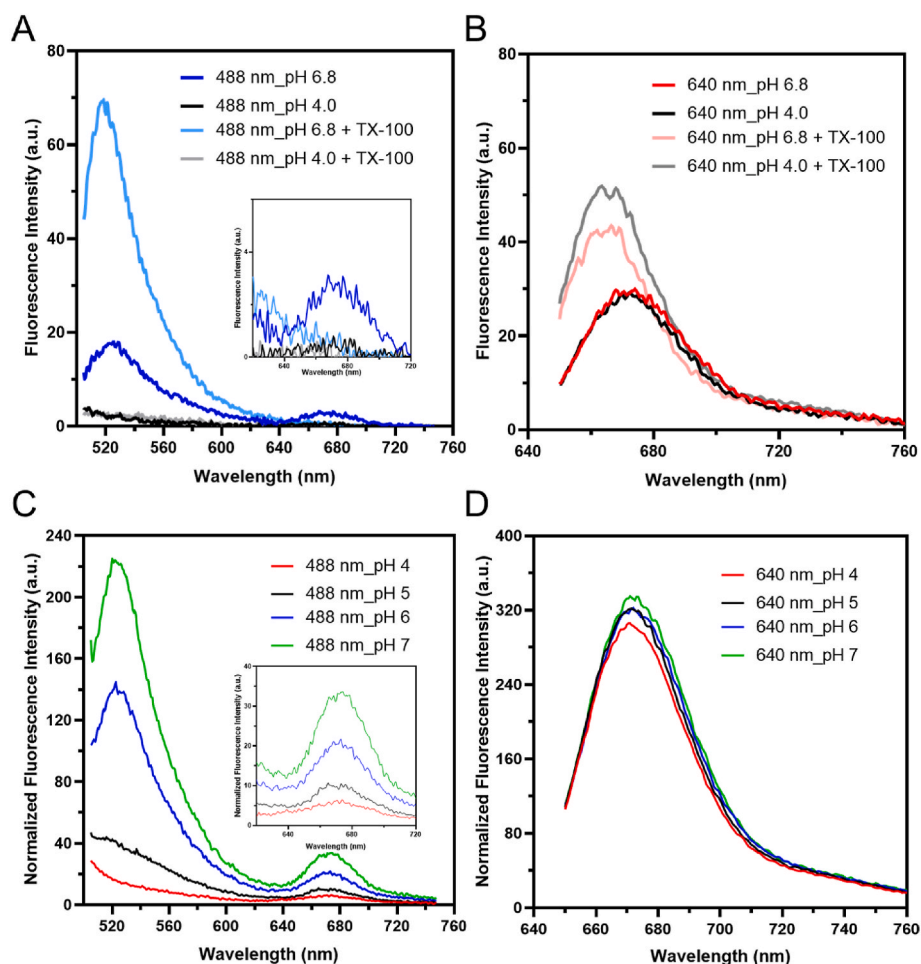


**Fig. 2.** Signal activation of DNA probes in LNP-siRNA&DNA. (A, B) Fluorescence emission spectra of DNA probes in LNP-siRNA&DNA at pH 4 and 6.8, when excited at 488 nm (A) and 640 nm (B). The fluorescent behavior of these samples following the addition of 1 % Triton X-100 (TX-100) was also shown. (C, D) Fluorescence emission spectra of DNA probes in LNP-siRNA&DNA dialyzed against citrate-phosphate buffer (containing 150 mM NaCl) at variable pHs, when excited at 488 nm (C) and 640 nm (D). Fluorescence intensity was normalized based on the lipid concentration.

originated from the inter-probe interaction inside the LNPs. Upon 640 nm excitation, emission peaks of Alexa Fluor 647 at 670 nm were detected for particles in both pH 4 and 6.8 buffer, and the intensities of the signals were comparable (Fig. 2B), likely because the Alexa Fluor 647 fluorophore was insensitive to pH changes. Increasing signal intensities together with a blue shift in the emission peak of Alexa Fluor 647 were observed under both pH conditions with Triton X-100 treatment.

We next tested the pH probe in LNPs formulated and dialyzed under different buffer conditions. LNP-siRNA&DNA were formulated in NaOAc-NaCl pH 4 or NaCl-free NaOAc pH 4 buffer, followed by dialysis against PBS. The activation of 6-FAM to produce a fluorescence signal at 520 nm and the corresponding FRET peaks were observed for both particles (Figure S4). Triton X-100 treatment further confirmed that the FRET signals resulted from the interaction of the two probes inside the LNPs. We also tested the probe with LNP-siRNA&DNA (formulated in NaOAc-NaCl pH 4 buffer) dialyzed against citrate-phosphate buffer at various pHs ranging from 4 to 7 (Fig. 2C and D). As the pH increased, the emission signals of 6-FAM and the FRET signals both increased, indicating that the probe's activation was dependent on the external buffer pH and that the internal core of the LNPs had the same pH as the external buffer. Also, the signal ratio of 6-FAM to Alexa Fluor 647 correlated well with the external buffer pH (Figure S5). The fluorescence ratio of 6-FAM to Alexa Fluor 647 was dramatically elevated by 12-fold (signal-to-noise ratio (S/N) = 11.9) as the pH increased from 4 to 7. It showed a wide dynamic range from pH 4 and 7 with a good linear relationship ( $R^2 = 0.97$ ). These results support the conclusion that the dual-labeled fluorescent DNA probe could serve as a ratiometric probe to determine the

internal pH of LNPs. Of note, the sensitivity (S/N) of the encapsulated pH-responsive DNA probes for LNP internal pH sensing is comparable to or superior to existing DNA-based pH sensors (Table S1) (Huang et al., 2015; Leung et al., 2019; Yue et al., 2021; Zhou et al., 2019).

### 3.3. Influence of acidification on pre-activated LNP-siRNA&DNA

To determine the response of the encapsulated pH probe to decreases in the external pH, LNP-siRNA&DNA samples prepared in NaOAc-NaCl pH 4 buffer were first activated by a 10-fold PBS dilution to achieve a final pH of 6.8. By simply adding a small volume of hydrochloric acid (HCl), the buffer pH was then lowered to 4, while the total volume of samples only increased by 6%. As expected, we detected a small decrease (~10%) in the signal of Alexa Fluor 647 at 670 nm (Fig. 3B). In contrast, as shown in Fig. 3A, a dramatic decrease in the 6-FAM (~6.2-fold decrease in the 520 nm peak signal) and the FRET signal (~2.7-fold decrease in 670 nm FRET peak) was observed.

We also lowered the pH from 6.8 to 5 by diluting the activated LNP sample 5-fold with the NaOAc-NaCl pH 4 buffer. When excited with light at 488 nm, 6-FAM showed a 22-fold signal reduction in the emission peak at 520 nm (Fig. 3C). The FRET signals displayed a 14-fold decrease in the 670 nm peak. The factors by which both signals decreased were significantly larger than the dilution factor of 5. Only a 4.6-fold decrease in the Alexa Fluor 647 signal at 670 nm was detected, which could be attributed to the change in volume (Fig. 3D). Another way to decrease the pH would be to re-dialyze the LNP-siRNA&DNA originally dialyzed against PBS with NaOAc-NaCl pH 4 buffer. Results showed that no 6-FAM and FRET signals were detected after the re-dialysis step

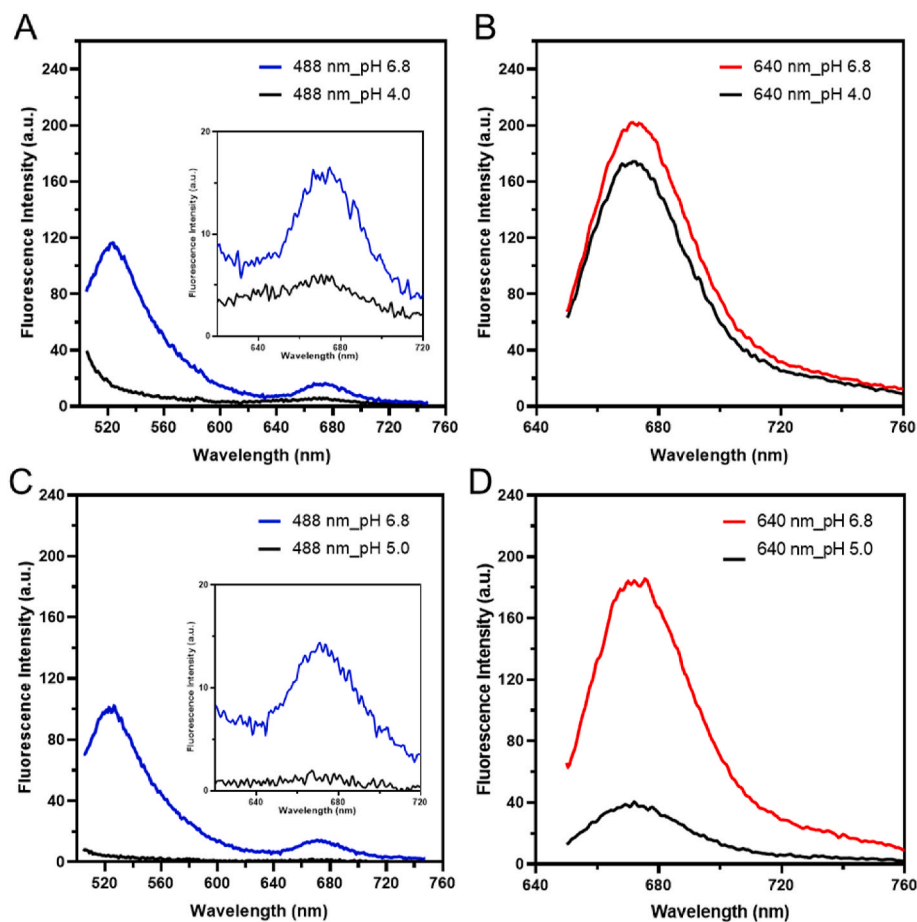


Fig. 3. Monitoring the acidification of the inside of pre-activated LNP-siRNA&DNA. (A, B) Fluorescence emission spectra of DNA probes in pre-activated LNP-siRNA&DNA with the addition of HCl, when excited at 488 nm (A) and 640 nm (B). (C, D) Fluorescence emission spectra of DNA probes in pre-activated LNP-siRNA&DNA upon a 5-fold dilution with NaOAc-NaCl pH 4 buffer, when excited at 488 nm (C) and 640 nm (D).

(Figure S6). There was no difference between re-dialyzed LNPs and LNPs directly dialyzed against NaOAc-NaCl pH 4 buffer. The results demonstrate that activation of the probe encapsulated in LNPs is fully reversible and that decreases in the external pH corresponds to decreases in the internal pH of the LNPs. The producibility of the encapsulated fluorescent DNA pH probe for monitoring LNP internal pH change was evaluated by repeating the experiments five times with five independent LNP formulations. A great producibility was observed for the acidification test (HCl addition or dilution with NaOAc-NaCl pH 4 buffer), as well as the aforementioned pH increase test (dilution with PBS) (Figure S7).

### 3.4. CLiC imaging of LNP-siRNA&DNA at a single particle scale

To further characterize the properties of the pH-sensitive probe, we investigated whether we could visualize pH changes in single LNPs using CLiC microscopy. CLiC microscopy is an emerging single molecule/particle imaging technique (Leslie et al., 2010), which enables simultaneous size and drug-loading measurements for individual LNP (Kamanzi et al., 2021). The weight ratio of siRNA and the DNA pH probe co-encapsulated in the LNPs was first optimized to achieve a good S/N for 6-FAM imaging (Figure S8), keeping the total weight of siRNA and DNA probe constant to ensure an amine-to-phosphate (N/P) ratio of 3. For LNPs containing siRNA and DNA probe at a 9:1 wt ratio, few particles were observed in the 6-FAM channel (green) due to the relatively low loading of 6-FAM. When the weight ratio of siRNA and DNA probe was adjusted to 1:1, a good number of particles were visible in both the Alexa Fluor 647 and the 6-FAM channel. LNPs containing siRNA and DNA probe at 1:1 ratio, denoted as LNP-siRNA&DNA (1:1), were therefore chosen for the CLiC imaging study.

The LNP-siRNA&DNA (1:1) sample was imaged before and after buffer exchange which could increase the pH from 4 to 7.4 (Fig. 4). Before the buffer exchange, the green channel exhibited very low fluorescence signals from the 6-FAM (Fig. 4 A-ii)), while the red channel showed strong signals from the Alexa Fluor 647 (Fig. 4 B-ii)). However, after buffer exchange, a large number of single LNPs with intense 6-FAM signals in the green channel were observed (Fig. 4 A-iv)). The Alexa Fluor 647 signal remained consistently strong (Fig. 4 B-iv)). This was further demonstrated by plotting histograms of mean intensities per CLiC micro-well, for the different imaging conditions used. Fig. 4 A-i) and A-iii) show significant shifts in the resulting histogram plots, with

approximately 5-fold increase in the mean fluorescence signals measured (from  $5.3 \pm 0.2$  to  $23.4 \pm 3.8$  electrons). In contrast, the measured fluorescence of Alexa Fluor 647 (Fig. 4 B-i) and B-iii)) remains relatively constant ( $13.8 \pm 3.5$  to  $15.9 \pm 4.3$  electrons). Time-lapse imaging allowed us to study the dynamics of the probes' activation when the single LNPs were subjected to buffer exchange, showing that the 6-FAM signal increased within  $271 \pm 165$  s (Supplementary Videos, Figure S9).

Lastly, we performed CLiC imaging on the probe encapsulated inside the LNPs formed in the presence of NaOAc pH 4 buffer and then dialyzed against PBS (denoted as Onpattro LNP-siRNA&DNA (1:1)) to observe pH-dependent changes in the fluorescence intensity. In this commonly used formulation process (Kulkarni et al., 2018), small vesicles were formed during the mixing of lipids with the NaOAc pH 4 buffer, and these vesicles would subsequently fuse to form larger structures when dialyzed against PBS (pH 7.4). This process is driven by the deprotonation of ionizable lipids and the resultant loss of charge which causes them to fall out of solution. DNA probes and siRNA at a 1:1 ratio (w/w) in the NaOAc pH 4 buffer were mixed with an ethanol solution of the lipids (Onpattro lipid composition) to produce a dispersion of small vesicles at pH 4 (Figure S10). Buffer exchange with PBS was then performed to form the Onpattro LNP-siRNA&DNA (1:1) (Figure S10). The pH probe signals were visualized using CLiC imaging before and after buffer exchange (Fig. 5). At pH 4 only a few particles were observed in the green channel due to the weak signal of 6-FAM at low pH (Fig. 5A-ii)). When the pH was raised to pH 7.4, a strong 6-FAM signal was observed as the small vesicles coalesced into larger LNPs (Fig. 5A-iv)). By contrast, the fluorescence of Alexa Fluor 647 from single particles remained consistently strong in the red channel before and after buffer exchange (Fig. 5B-ii)&iv)). Histograms of fluorescence intensities of 6-FAM per micro-wells (Fig. 5A-i)&iii)) displayed a significant increase in the average 6-FAM signal of single LNPs after buffer exchange (from  $4.1 \pm 0.6$  to  $16.9 \pm 4.2$  electrons), while no change was observed for the Alexa Fluor 647 signal (Fig. 5B-i)&iii)),  $15.2 \pm 3.2$  electrons vs  $15.4 \pm 3.4$  electrons). These results support the conclusion that the pH in the interior core of LNP RNA systems containing ionizable lipids reflects the exterior pH no matter which formulation technique is employed.

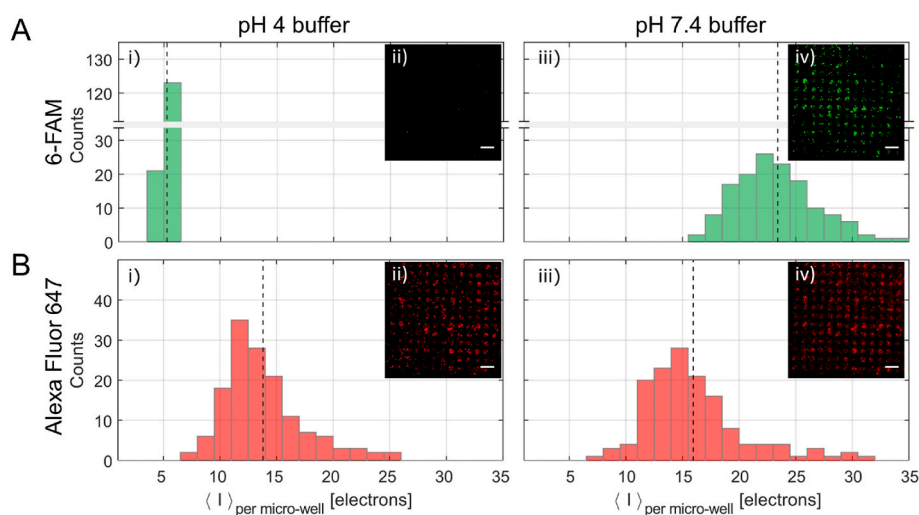


**Fig. 4.** CLiC imaging of LNP-siRNA&DNA (1:1) before and after buffer exchange. (A) Representative image of LNPs in the 6-FAM channel and histograms of fluorescence intensities per micro-wells before (pH 4, i)&ii)) and after (pH 7.4, iii)&iv)) buffer exchange. The dotted lines in i) and iii) indicate the mean fluorescence intensities per micro-wells before and after buffer exchange, which are  $5.3 \pm 0.2$  electrons and  $23.4 \pm 3.8$  electrons respectively. Scale bar = 10  $\mu$ m. (B) Representative image of the same LNPs in the Alexa Fluor 647 channel and histograms of fluorescence intensities per micro-wells before (pH 4, i)&ii)) and after (pH 7.4, iii)&iv)) buffer exchange. The dotted lines in i) and iii) indicate the mean fluorescence intensities per micro-wells before and after buffer exchange, which are  $13.8 \pm 3.5$  electrons and  $15.9 \pm 4.3$  electrons respectively. Scale bar = 10  $\mu$ m.

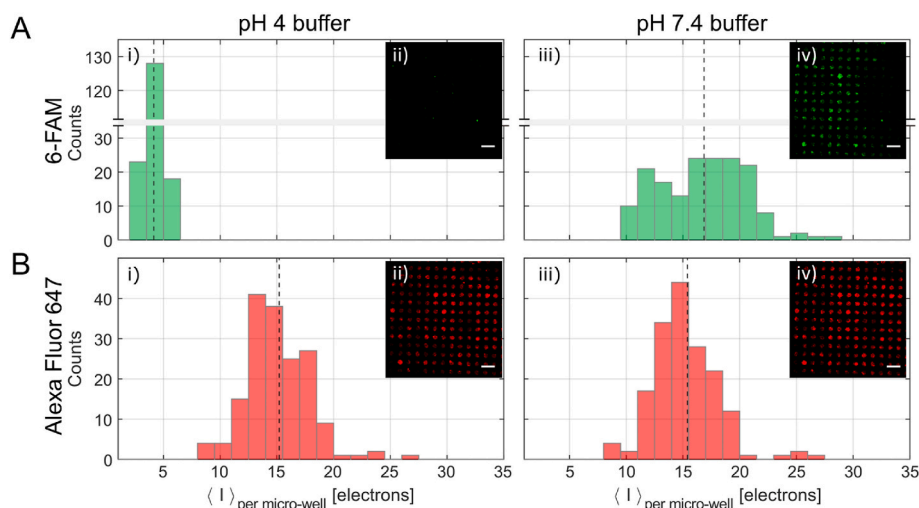


**Fig. 5.** CLiC imaging of Onpattro LNP-siRNA&DNA (1:1) before and after buffer exchange. (A) Representative image of LNPs in the 6-FAM channel and histograms of fluorescence intensities per micro-wells before (pH 4, i)&ii) and after (pH 7.4, iii)&iv)) buffer exchange. The dotted lines in i) and iii) indicate the mean fluorescence intensities per micro-wells before and after buffer exchange, which are  $4.1 \pm 0.6$  electrons and  $16.9 \pm 4.2$  electrons respectively. Scale bar = 10  $\mu\text{m}$ . (B) Representative image of the same LNPs in the Alexa Fluor 647 channel and histograms of fluorescence intensities per micro-wells before (pH 4, i)&ii) and after (pH 7.4, iii)&iv)) buffer exchange. The dotted lines in i) and iii) indicate the mean fluorescence intensities per micro-wells before and after buffer exchange, which are  $15.2 \pm 3.2$  electrons and  $15.4 \pm 3.4$  electrons respectively. Scale bar = 10  $\mu\text{m}$ .

#### 4. Discussion

There are two important findings from this work. First, the pH-responsive DNA probe that was developed could be used to directly monitor the internal pH of LNP systems containing ionizable cationic lipids, and that the internal pH of the LNP systems with the Onpattro lipid composition mirrored the external pH. This finding implies that the internal pH of LNP RNA formulations approved clinically, such as Onpattro and Comirnaty, likely reflects the external pH of 7.4, consistent with how the ionizable lipid is in a neutral “solid oil core” form (Kulkarni et al., 2018). This is also consistent with a recent study on Comirnaty LNPs that reported that there was no pH gradient between the LNP core and the external medium (Szebeni et al., 2023). Second, the FRET signal observed in this study is of particular interest as it supports a model where the encapsulated nucleic acid is sequestered at high concentrations into a polar compartment within the LNPs at pH 7.4. The data presented supports the model shown in Figure S11. At pH 4, there was no detectable FRET between 6-FAM and Alexa Fluor 647 due to the inactive state of 6-FAM. When the pH was raised to 7.4, 6-FAM was activated, enabling efficient inter-probe FRET of 6-FAM and Alexa Fluor 647 due to the proximity of the two dyes. Furthermore, FRET signals were dependent on the activation of 6-FAM and increased as the pH increased. When the pH was brought back to 4, 6-FAM returned to the inactive state, disabling the intermolecular FRET. This FRET signal implies a high concentration of encapsulated nucleic acids in polar regions of the LNP formulations at physiological pH, which is consistent with the proposed morphology such as inverted micelles (Leung et al., 2012) or “bleb” (Cheng et al., 2023) structures that contain encapsulated siRNA or mRNA.

Compared to existing pH-sensitive fluorescent dyes, our rationally designed dual-labeled fluorescent DNA pH probe has several unique features. First, the use of a short DNA duplex (41 base pair) as a carrier of the pH-sensitive dye (6-FAM) and a mimic of siRNA is capable of encapsulating the dye into the LNP core specifically and therefore allowing for the monitoring of the pH microenvironment that ionizable lipids in LNPs are exposed to. In contrast, free pH-sensitive dyes cannot be specifically entrapped into the core of LNPs. Second, DNA can be cost-effectively synthesized and covalently conjugated with fluorophores in a single step. The covalent chemical conjugation of the DNA duplex with the 6-FAM and Alexa Fluor 647 could help anchor the dyes in the LNP

core and prevent their leakage out of LNPs. Without such chemical conjugation, free cell dyes (pH sensitive or insensitive) can easily leak out of LNPs. Third, thanks to the stoichiometry of DNA hybridization (Leung et al., 2019), we incorporated the pH-sensitive fluorescent dye (6-FAM) and an internal reference dye (Alexa Fluor 647) to yield a ratiometric probe with a precise 1:1 stoichiometry. It holds great promise for practical applications of the probe for quantitatively measuring the interior pH of LNPs along endocytic pathways in living cells. However, free pH-sensitive dyes themselves lack the ability for precise quantification of pHs in LNPs or cells.

To the best of our knowledge, this work represents the first integration of a pH-responsive DNA nanoprobe into ionizable LNPs for direct determination of the interior pH of ionizable LNPs. The developed pH-sensitive dye-based fluorescent DNA sensor exhibits a wide working range, high sensitivity, and unique ability of sensing the pH of solid cores of ionizable LNPs (Table S1). Furthermore, the pH-sensitive DNA probe can be encapsulated into ionizable LNPs at levels sufficient, which allows for direct visualization of the internal pH of single LNPs by CLiC imaging.

#### 5. Conclusions

In summary, we reported a dual-label fluorescent DNA pH probe which could be readily integrated into ionizable LNPs for the pH sensing purpose. The capability of the probe to determine the interior pH of ionizable LNPs has been demonstrated in bulk solution or at a single particle scale. The results of this investigation indicate that the ionizable lipids in the LNP RNA formulations experience a pH consistent with the adoption of a neutral form at physiological values. It is anticipated that this work will pave the way for applying functional nucleic acids and complex DNA nanostructures into LNPs for sensing, imaging and biomedical applications.

#### CRedit authorship contribution statement

**Bin Zhao:** Writing – original draft, Visualization, Validation, Supervision, Methodology, Investigation, Conceptualization. **Albert Kamanzi:** Writing – review & editing, Visualization, Validation, Investigation. **Yao Zhang:** Writing – review & editing, Visualization, Investigation. **Karen Y.T. Chan:** Writing – review & editing, Data curation.

**Madelaine Robertson:** Writing – review & editing, Validation. **Sabrina Leslie:** Writing – review & editing, Resources, Data curation. **Pieter R. Cullis:** Writing – review & editing, Supervision, Resources, Project administration, Funding acquisition, Data curation, Conceptualization.

#### Declaration of competing interest

The authors declare the following financial interests/personal relationships which may be considered as potential competing interests: Pieter R. Cullis has a financial interest in Acuitas Therapeutics and NanoVation Therapeutics. He is the Chair of NanoVation Therapeutics. If there are other authors, they declare that they have no known competing financial interests or personal relationships that could have appeared to influence the work reported in this paper.

#### Data availability

The data that has been used is confidential.

#### Acknowledgements

Grids were prepared and data collected at the High Resolution Macromolecular Electron Microscopy (HRMEM) facility at the University of British Columbia (<https://cryoem.med.ubc.ca>). We thank Claire Atkinson, Joeseeph Felt, Liam Worrall and Natalie Strynadka. HRMEM is funded by the Canadian Foundation for Innovation and the British Columbia Knowledge Development Fund. We also thank members of the NanoMedicines Research Group for useful discussions. This work was funded by the Canadian Institutes of Health Research (CIHR) through grant FN 148469.

#### Appendix A. Supplementary data

Supplementary data to this article can be found online at <https://doi.org/10.1016/j.bios.2024.116065>.

#### References

- Adams, D., Gonzalez-Duarte, A., O’Riordan, W.D., Yang, C.-C., Ueda, M., Kristen, A.V., Tournev, I., Schmidt, H.H., Coelho, T., Berk, J.L.J.N.E.J.o.M., 2018. *N. Engl. J. Med.* 379 (1), 11–21.
- Akinc, A., Maier, M.A., Manoharan, M., Fitzgerald, K., Jayaraman, M., Barros, S., Ansell, S., Du, X., Hope, M.J., Madden, T.D., Mui, B.L., Semple, S.C., Tam, Y.K., Ciufolini, M., Witzigmann, D., Kulkarni, J.A., van der Meel, R., Cullis, P.R., 2019. *Nat. Nanotechnol.* 14 (12), 1084–1087.
- Amodio, A., Zhao, B., Porchetta, A., Idili, A., Castronovo, M., Fan, C., Ricci, F., 2014. *J. Am. Chem. Soc.* 136 (47), 16469–16472.
- Batzri, S., Korn, E.D., 1973. *Biochim. Biophys. Acta* 298 (4), 1015–1019.
- Cheng, M.H.Y., Brimacombe, C.A., Verbeke, R., Cullis, P.R., 2022. *Mol. Pharm.* 19 (6), 1663–1668.
- Cheng, M.H.Y., Leung, J., Zhang, Y., Strong, C., Basha, G., Momeni, A., Chen, Y., Jan, E., Abdolazadeh, A., Wang, X., Kulkarni, J.A., Witzigmann, D., Cullis, P.R., 2023. *Adv. Mater.* 35 (31), 2303370.
- Emilsson, G., Schoch, R.L., Feuz, L., Höök, F., Lim, R.Y.H., Dahlin, A.B., 2015. *ACS Appl. Mater. Interfaces* 7 (14), 7505–7515.
- Gilleron, J., Querbes, W., Zeigerer, A., Borodovsky, A., Marsico, G., Schubert, U., Manygoats, K., Seifert, S., Andree, C., Stöter, M., Epstein-Barash, H., Zhang, L., Koteliangsky, V., Fitzgerald, K., Fava, E., Bickle, M., Kalaidzidis, Y., Akinc, A., Maier, M., Zerial, M., 2013. *Nat. Biotechnol.* 31 (7), 638–646.
- Hafez, I.M., Maurer, N., Cullis, P.R., 2001. *Gene Ther.* 8 (15), 1188–1196.
- Han, X., Zhang, H., Butowska, K., Swingle, K.L., Alameh, M.-G., Weissman, D., Mitchell, M.J., 2021. *Nat. Commun.* 12 (1), 7233.
- Henkin, G., Berard, D., Stabile, F., Shayegan, M., Leith, J.S., Leslie, S.R., 2016. *Anal. Chem.* 88 (22), 11100–11107.
- Hu, B., Zhong, L., Weng, Y., Peng, L., Huang, Y., Zhao, Y., Liang, X.-J., 2020. *Signal Transduct. Targeted Ther.* 5 (1), 101.
- Huang, G., Su, C., Wang, L., Fei, Y., Yang, J., 2021. *Front. Chem.* 9, 705458.
- Huang, J., Ying, L., Yang, X., Yang, Y., Quan, K., Wang, H., Xie, N., Ou, M., Zhou, Q., Wang, K., 2015. *Anal. Chem.* 87 (17), 8724–8731.
- Juskowiak, B., 2011. *Anal. Bioanal. Chem.* 399 (9), 3157–3176.
- Kamanzi, A., Gu, Y., Tahvildari, R., Friedenberger, Z., Zhu, X., Berti, R., Kurylowicz, M., Witzigmann, D., Kulkarni, J.A., Leung, J., Andersson, J., Dahlin, A., Höök, F., Sutton, M., Cullis, P.R., Leslie, S., 2021. *ACS Nano* 15 (12), 19244–19255.
- Keshri, P., Zhao, B., Xie, T., Bagheri, Y., Chambers, J., Sun, Y., You, M., 2021. *Angew. Chem., Int. Ed.* 60 (28), 15548–15555.
- Kulkarni, J.A., Darjuan, M.M., Mercer, J.E., Chen, S., Van Der Meel, R., Thewalt, J.L., Tam, Y.Y.C., Cullis, P.R.J.A.n., 2018. *ACS Nano* 12 (5), 4787–4795.
- Kulkarni, J.A., Witzigmann, D., Chen, S., Cullis, P.R., van der Meel, R., 2019a. *Acc. Chem. Res.* 52 (9), 2435–2444.
- Kulkarni, J.A., Witzigmann, D., Leung, J., van der Meel, R., Zaifman, J., Darjuan, M.M., Grisch-Chan, H.M., Thöny, B., Tam, Y.Y.C., Cullis, P.R., 2019b. *Nanoscale* 11 (18), 9023–9031.
- Le Guern, F., Müssard, V., Gaucher, A., Rottman, M., Prim, D., 2020. *Int. J. Mol. Sci.* 21 (23), 9217.
- Leslie, S.R., Fields, A.P., Cohen, A.E., 2010. *Anal. Chem.* 82 (14), 6224–6229.
- Leung, A.K.K., Hafez, I.M., Baoukina, S., Belliveau, N.M., Zhigaltsev, I.V., Afshinmanesh, E., Tieleman, D.P., Hansen, C.L., Hope, M.J., Cullis, P.R., 2012. *J. Phys. Chem. C* 116 (34), 18440–18450.
- Leung, A.K.K., Tam, Y.Y.C., Chen, S., Hafez, I.M., Cullis, P.R., 2015. *J. Phys. Chem. B* 119 (28), 8698–8706.
- Leung, K., Chakraborty, K., Saminathan, A., Krishnan, Y., 2019. *Nat. Nanotechnol.* 14 (2), 176–183.
- Modi, S., M. G. S., Goswami, D., Gupta, G.D., Mayor, S., Krishnan, Y., 2009. *Nat. Nanotechnol.* 4 (5), 325–330.
- Modi, S., Nizak, C., Surana, S., Halder, S., Krishnan, Y., 2013. *Nat. Nanotechnol.* 8 (6), 459–467.
- Semple, S.C., Akinc, A., Chen, J., Sandhu, A.P., Mui, B.L., Cho, C.K., Sah, D.W.Y., Stebbing, D., Crosley, E.J., Yaworski, E., Hafez, I.M., Dorkin, J.R., Qin, J., Lam, K., Rajeev, K.G., Wong, K.F., Jeffs, L.B., Nechev, L., Eisenhardt, M.L., Jayaraman, M., Kazem, M., Maier, M.A., Srinivasulu, M., Weinstein, M.J., Chen, Q., Alvarez, R., Barros, S.A., De, S., Klimuk, S.K., Borland, T., Kosovrasti, V., Cantley, W.L., Tam, Y.K., Manoharan, M., Ciufolini, M.A., Tracy, M.A., de Fougères, A., MacLachlan, I., Cullis, P.R., Madden, T.D., Hope, M.J., 2010. *Nat. Biotechnol.* 28 (2), 172–176.
- Sun, D., Lu, Z.-R., 2023. *Pharm. Res. (N. Y.)* 40 (1), 27–46.
- Szebeni, J., Kiss, B., Bozó, T., Turjeman, K., Levi-Kalishman, Y., Barenholz, Y., Kellermayer, M., 2023. *ACS Nano* 17 (14), 13147–13157.
- Witzigmann, D., Kulkarni, J.A., Leung, J., Chen, S., Cullis, P.R., van der Meel, R., 2020. *Adv. Drug Deliv. Rev.* 159, 344–363.
- Yue, X., Qiao, Y., Gu, D., Qi, R., Zhao, H., Yin, Y., Zhao, W., Xi, R., Meng, M., 2021. *Anal. Chem.* 93 (19), 7250–7257.
- Zhao, B., O’Brien, C., Mudiyansele, A.P.K.K.K., Li, N., Bagheri, Y., Wu, R., Sun, Y., You, M., 2017. *J. Am. Chem. Soc.* 139 (50), 18182–18185.
- Zheng, L., Bandara, S.R., Tan, Z., Leal, C., 2023. *Proc. Natl. Acad. Sci. U. S. A.* 120 (27), e2301067120.
- Zhou, Y.-J., Wan, Y.-H., Nie, C.-P., Zhang, J., Chen, T.-T., Chu, X., 2019. *Anal. Chem.* 91 (16), 10366–10370.